

Study of the Effective Torus Exhaust High Vacuum Pumping System Performance in the Inner Tritium Plant Loop of EU-DEMO

Tim Teichmann, Xueli Luo, Thomas Giegerich & Christian Day

To cite this article: Tim Teichmann, Xueli Luo, Thomas Giegerich & Christian Day (23 Aug 2023): Study of the Effective Torus Exhaust High Vacuum Pumping System Performance in the Inner Tritium Plant Loop of EU-DEMO, Fusion Science and Technology, DOI: [10.1080/15361055.2023.2229679](https://doi.org/10.1080/15361055.2023.2229679)

To link to this article: <https://doi.org/10.1080/15361055.2023.2229679>



© 2023 The Author(s). Published with license by Taylor & Francis Group, LLC.



Published online: 23 Aug 2023.



Submit your article to this journal [↗](#)



Article views: 273



View related articles [↗](#)



View Crossmark data [↗](#)



Study of the Effective Torus Exhaust High Vacuum Pumping System Performance in the Inner Tritium Plant Loop of EU-DEMO

Tim Teichmann,^{✉*} Xueli Luo, Thomas Giegerich, and Christian Day

Karlsruhe Institute of Technology (KIT), Institute for Technical Physics (ITEP), Hermann-von-Helmholtz-Platz 1, 76344 Eggenstein-Leopoldshafen, Germany

Received January 31, 2023

Accepted for Publication June 21, 2023

Abstract — *The requirement for a reduction of the tritium inventory of the European demonstration fusion reactor (EU-DEMO) has led to the active research and development of a continuously working pumping process termed “KALPUREX.” This process foresees the direct recycling of a large fraction of the unburnt hydrogen isotopologues via superpermeation in metal foil pumps during the burn phase. The remaining exhaust gas mixture is pumped by continuously operating, mercury-driven linear diffusion pumps. Diffusion pumps are kinetic high vacuum pumps whose pumping principle is based on the momentum transfer from a supersonic mercury vapor jet to the pumped gas mixture. Like many high vacuum pumps, they feature species-dependent pumping speeds. In the present work, we develop a simplified hybrid model of the high vacuum pumping train in order to estimate the effective pumping speed of the integrated system. The results of this model and its implications on the further development of the vacuum system are discussed for the burn and dwell phases of EU-DEMO.*

Keywords — *Fusion reactor, torus exhaust pumping, high vacuum.*

Note — *Some figures may be in color only in the electronic version.*

I. INTRODUCTION

Unburnt fuel, composed of the hydrogen isotopologues Q_2 ,^a makes up for about 98% of the exhaust gas mixture. The remaining about 2% is mainly comprised of helium, the ash of the fusion reaction, and plasma enhancement gases (PEGs), like xenon or argon (in EU-DEMO). Furthermore, small quantities of other impurities, like water (Q_2O) and hydrocarbons (e.g., CQ_4), are expected in the exhaust gas mixture. The exact

composition is not known at this time and is subject to change due to design and operating condition changes.

The exhaust gases are extracted from the fusion reactor torus via pumping ports that are attached below the divertor (DIV). Because of the large amount of unburnt fuel, it is very beneficial to recycle a large fraction of it directly, a concept termed direct internal recycling (DIR).^[1] The KALPUREX process is an implementation of the DIR concept using metal foil pumps (MFPs) for separation and primary pumping of the unburnt fuel and mercury-driven linear diffusion pumps (LDPs) for the primary pumping of the remaining part of the exhaust gases.^[2–4] A combination of mercury-driven booster pumps and liquid ring pumps is used as backing pumps (BPs). The separation of the exhaust gas mixture results in two loops that are referred to as the direct internal recycling loop (DIRL) for the recycled stream carrying pure hydrogenic species and the inner tritium plant loop (INTL) for the unseparated stream.^[4] An overview of the system is depicted in Fig. 1.

*E-mail: tim.teichmann@kit.edu

This is an Open Access article distributed under the terms of the Creative Commons Attribution-NonCommercial-NoDerivatives License (<http://creativecommons.org/licenses/by-nc-nd/4.0/>), which permits non-commercial re-use, distribution, and reproduction in any medium, provided the original work is properly cited, and is not altered, transformed, or built upon in any way. The terms on which this article has been published allow the posting of the Accepted Manuscript in a repository by the author(s) or with their consent.

^a The abbreviation $Q_2 = \{H_2, HD, HT, D_2, DT, T_2\}$ is used.

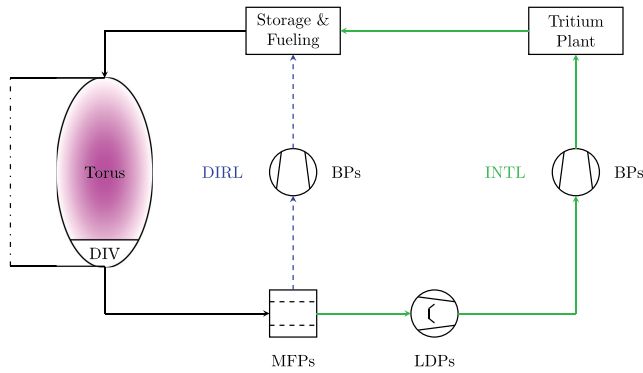


Fig. 1. Simplified sketch of the KALPUREX exhaust pumping process (based on Refs. [2,3,4]). Abbreviations of the subsystems are explained in the text. The flow in the DIRT (dashed) is only active during the burn phase.

During the burn phase, both loops are active and the flow rate in the DIRT is higher than in the INTL. However, during the dwell phase, the MFPs are not operated, and therefore, the dwell pumping is supplied by the high vacuum system of the INTL. The present work aims to build a simplified model of the high vacuum system of the INTL. The central idea is to combine sophisticated models for the individual subsystems in the form of a hybrid model to estimate the integrated performance. This is extremely important to identify optimization potentials in the system during operation of the fusion reactor. While the vacuum system has to fulfill several roles, e.g., during off-normal events and maintenance, we focus on the two most important operating states (i.e., plasma burn and dwell phases) in the present work.

II. THEORY AND METHOD

II.A. Vacuum Terminology and Definitions

High vacuum pumps are characterized by the so-called pumping speed S , which corresponds to the volumetric flow rate that is pumped through the inlet of the pump. Another commonly used quantity is the dimensionless capture coefficient ζ ,^[5] which is defined as

$$\zeta = \frac{4 \cdot S}{A_{\text{in}} \cdot v_{\text{th}}} = \frac{4 \cdot \dot{N} \cdot k_B \cdot T}{A_{\text{in}} \cdot v_{\text{th}} \cdot p_{\text{in}}}, \quad (1)$$

where

- \dot{N} = pumped number flow rate
- A_{in} = inlet cross section of the pump
- k_B = Boltzmann constant

T = temperature

p_{in} = pressure in the recipient

$$v_{\text{th}} = \sqrt{\frac{8 \cdot k_B \cdot T}{\pi \cdot m}} = \text{thermal velocity of the gas with molecular mass } m.$$

For many high vacuum pumps, the pumping speed and capture coefficient are approximately constant for a given gas species irrespective of the chosen BP and for a wide range (order of magnitudes) of inlet pressures.

The available pumping speed or capture coefficient at an arbitrarily chosen cross section in the vacuum system connected to a vacuum pump is referred to as the effective pumping speed or capture coefficient. It is by definition smaller than the nominal pumping speed of the pump due to the limited conductance C of the piping. Similar to the pumping speed, the conductance corresponds to a volumetric flow rate. Its dimensionless counterpart is called transmission probability ω and is defined as

$$\omega = \frac{4 \cdot C}{A_{\text{in}} \cdot v_{\text{th}}} = \frac{4 \cdot \dot{N}_0 \cdot k_B \cdot T}{A_{\text{in}} \cdot v_{\text{th}} \cdot p_{\text{in}}}. \quad (2)$$

The important distinction to the capture coefficient [see Eq. (1)] is that the transmission probability is calculated under the assumption that a perfect vacuum pump, responsible for the flow rate \dot{N}_0 , is connected to the outlet of the system. Analytical expressions for the transmission probability exist only for very simple components, e.g., circular tubes. For geometrically complex structures (e.g., the EU-DEMO pumping duct), the standard procedure is to use the “test particle Monte Carlo” (TPMC) method, which works by tracing computational test particles through the component and simulating their interaction with the walls. Each simulated particle will either leave the component through the inlet or outlet surfaces. The transmission probability is then readily computed as the ratio of particles pumped (counted at outlet) to injected particles. The results for standard components (e.g., elbows) are available in tabulated form in the literature.^[6] The TPMC method is based on the assumption that the gas is in the free molecular regime, thus neglecting intermolecular collisions. If this assumption is not valid, the “direct simulation Monte Carlo” (DSMC) method^[7] can be employed. Similar to TPMC, DSMC is a statistic particle method. However, intermolecular collisions are also considered by discretizing time and space.

II.B. Ansatz of Oatley

The effective capture coefficient of complex vacuum systems can either be determined by simulating the entire system or estimated based on the properties of the involved subsystems. While the former approach yields more accurate results, the latter has the distinct advantage that the subsystems can be simulated and optimized individually using smaller, more efficient models. The ‘‘Ansatz of Oatley’’ is an established method to estimate the effective capture coefficient of complex vacuum systems.^[8–11] Conceptually, the Ansatz of Oatley is similar to the regular treatment of a series connection of resistances (as known from electric circuits) with the important inclusion of the flow direction and the corresponding interface inflow resistances. The effective capture coefficient c_{eff} at the inlet of a complex vacuum system, which is composed of $N - 1$ subsystems and connected to a vacuum pump (subsystem N), can be estimated for an isothermal system using the generalized Ansatz of Oatley:

$$\frac{1}{A_{1,\text{in}}} \left(\frac{1}{c_{\text{eff}}} - 1 \right) = \sum_{i=1}^{N-1} \frac{1}{A_{i,\text{in}}} \left(\frac{1}{\omega_i} - 1 \right) + \frac{1}{A_{N,\text{in}}} \left(\frac{1}{c_N} - 1 \right) + \sum_{i=2}^N \frac{1}{A_{i-1,\text{out}}} \left(\max \left\{ \frac{A_{i-1,\text{out}}}{A_{i,\text{in}}}, 1 \right\} - 1 \right), \quad (3)$$

where $A_{i,\text{in}}$ and $A_{i,\text{out}}$ refer to the inlet and outlet cross sections of the individual subsystems, respectively. The first two terms on the right side account for the flow resistance of the involved subsystems. The last term on the right side of Eq. (3) accounts for reductions in the cross sections in the flow direction by considering them as orifices. Due to the assumptions made in the derivation of the Ansatz of Oatley, the subsystem transmission probabilities have to include the inflow resistance of the respective parts. In the free molecular regime, this corresponds to assuming a Maxwell-Boltzmann particle velocity distribution function at the inlet of the respective subsystems. Physically speaking, this corresponds to assuming that a large reservoir is connected at the inlet of the subsystem.

III. MODELING

III.A. Related Work and Overview

The Ansatz of Oatley and similar approaches are commonly used to describe complex vacuum systems.

In the context of nuclear fusion, ITERVAC has been used to describe the complex vacuum system of ITER as a network of interconnected simpler elements.^[12] For these simpler elements, semi-empirical relations are used to describe their conductance in all flow regimes. Recently, Karpov et al.^[13] used a similar approach to model the vacuum pumping system of tokamak with reactor technologies (TRT). The estimations in the aforementioned work were performed in the molecular regime, as the conductances are lower in that regime. Similar to ITERVAC, the complex conductance of the vacuum duct was estimated from expressions for simple elements.

Similar to Karpov et al.,^[13] we rely on a fully free molecular description of the integrated vacuum system in the present work, as this is considered to be conservative. However, we propose to use sophisticated simulation results (TPMC and DSMC) for entire subsystems instead of describing them as a collection of simpler geometric parts as has been done in the past. On the one hand, computational resources have become so cheap that TPMC simulations of even extremely complex three-dimensional geometries can now be performed in acceptable time spans. On the other hand, most of these simulations exist already because they are required to optimize the individual subsystems (e.g., baffles, pumps, etc.). For example, an initial study of the duct and MFP transmission probability was conducted in Giegerich et al.^[3] If not, at least three-dimensional computer-aided design (CAD) models usually exist for which TPMC simulations can be set up. The individual simulation models are then mathematically connected using the Ansatz of Oatley [Eq. (3)] to obtain a loosely coupled hybrid model of the whole pumping system that can be used to estimate the performance for different subsystem configurations and operating conditions.

III.B. Subsystems

An exploded three-dimensional CAD drawing of a single pumping port with an installed high vacuum pumping system is depicted in Fig. 2. The subsystems are indicated by the different colors. In the present work, we estimate the effective pumping speed at the inlet of the pumping duct. This implies that the conductance of the DIV is not considered here. Thus, the results are valid for the sub-DIV volume and not for the plasma chamber. In total, three subsystems were considered, each by an individual model. The first subsystem was composed of the pumping duct and the MFPs (see blue in Fig. 2). The second considered system was the mercury baffle adapter (MBA),

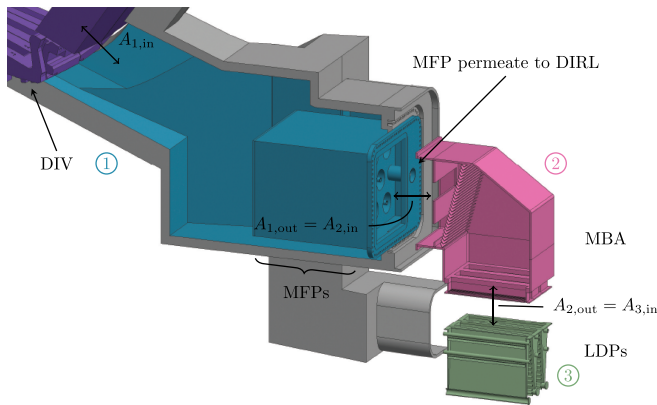


Fig. 2. Exploded and cut three-dimensional CAD model of the EU-DEMO high vacuum pumping system in an exemplary pumping port (preconceptual design state). Different colors are used for the subsystems: purple: DIV, blue: pumping duct and MFPs, pink: MBA, and green: LDPs.

(see pink in Fig. 2). The last system was comprised of three mercury-driven LDPs (see green in Fig. 2) in parallel. The following sections describe the models and results for the individual subsystems in more detail.

III.B.1. Duct and MFPs

The duct and MFPs were combined into a single model because the number and size of the MFPs is not yet fixed. Therefore, no straightforward interface between the duct and MFPs exists, where the geometry could be split. The MFP working principle is based on superpermeation of atomic hydrogen through a metal foil with a surface oxygen layer, with the atomic hydrogen produced on the upstream side using a plasma source.^[14] While not fixed, a cylindrical shape is currently assumed for the MFPs.^[3,15] The plasma source was represented by a small cylindrical tube in the centerline. In the present work, the number and size of MFPs was varied to test the impact of these changes on the performance. The three-dimensional model of the duct was slightly simplified by truncating the two vertical channels below the MFPs (only one is visible in Fig. 2 due to the cut).

The combination of duct and MFPs was simulated using the TPMC method. The transmission probability was derived by injecting test particles at the interface between the duct and sub-DIV volume based on a Maxwell-Boltzmann distribution function. At the interface between the MFPs and MBA, a sticking coefficient of unity was assigned. In the present work, we are only dealing with the INTL vacuum system. Therefore, it is legitimate to consider the cylindrical MFP membrane as an impermeable surface while reducing the throughput during

burn accordingly. (For the treatment of the DIRL, the reader is referred to Giegerich et al.^[3] where a similar approach has been used but with considering the membranes as permeable for hydrogenic species.) The simulations were performed using ProVac3D,^[3,16,17] which is an in-house, parallelized, validated, three-dimensional TPMC code. The relevant system dimensions, interfaces, and numerical results of the transmission probability are summarized in Table I.

III.B.2. Mercury Baffle Adapter

The MBA is located between the MFPs and the LDPs. It is responsible for mitigating the diffusion of mercury vapor against the main flow direction. For this reason, cooled baffles are installed in such a way that the direct line of sight between the MFP and LDP is blocked. In order to recycle as much mercury as possible, it is currently foreseen to include two baffle stages^[2]: the first baffle stage (from the LDP side) would be cooled to a temperature slightly above the mercury triple point at 234 K (e.g., 240 K) in order to condense incident mercury vapor. The second stage (farther away from the LDP) would be cooled to even lower temperatures (< 200 K) to sublimate the remaining mercury vapor. It is not yet fixed whether the first baffle stage will be integrated into the LDPs directly or be part of the MBA.

In the present study, both stages were considered in the numerical model of the MBA (see Fig. 2). As the MBA has to be regenerated within machine maintenance, a high vacuum valve is required to seal the MBA from the MFPs. In the preliminary design, this was considered as a gate valve upstream of the second baffle stage. Two different MBA configurations were investigated in the present work, with a comparison available in Fig. 3.

Figure 3a shows the MBA with classic, vertical mounting of the LDPs, which requires that the MBA include a 90-deg bend. We also investigate a second, optimized configuration, shown in Fig. 3b, where the LDPs are mounted in an inclined fashion. This removes the 90-deg bend and reduces the overall length of the flow path, which both contribute to an increase in conductance. The important properties of both configurations are listed in Table II. The transmission probability of both configurations was determined using the open-source, three-dimensional TPMC code MOLFLOW+.^[18] Particles were inserted at the MBA inlet based on a Maxwell-Boltzmann distribution function. It is noted that the simplified MBA configuration (Fig. 3b) leads to an increase in the transmission probability of about 6%.

TABLE I
Properties of the Subsystem Containing the Duct and MFPs for the Four Configurations Investigated

Property	Symbol	Unit	Configuration and Value			
			A	B	C	D
Inlet cross section (interface to DIV)	$A_{1,in}$	m ²	5.62			
Outlet cross section (interface to MBA)	$A_{1,out}$	m ²	3.04			
Diameter of plasma source	d	m	0.1			
Number of MFP tubes	N_{MFP}	1	8		6	
MFP diameter	D_{MFP}	m	0.25	0.45	0.25	0.45
Total MFP inlet cross section	A_{MFP}	m ²	0.330	1.21	0.247	0.907
Transmission probability (TPMC, ProVac3D)	ω_1	1	0.00481	0.0309	0.00362	0.0237

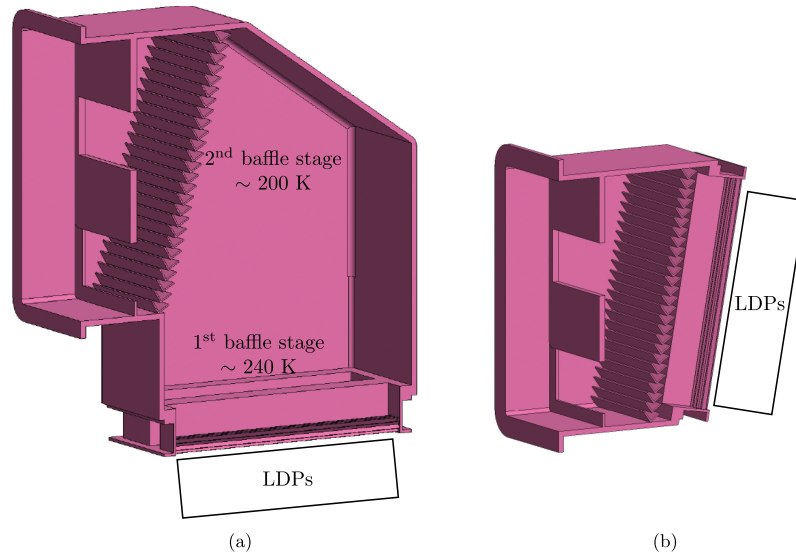


Fig. 3. Cut three-dimensional CAD model of the two preliminary MBA configurations: (a) LDPs mounted vertically and (b) LDPs mounted inclined.

III.B.3. Linear Diffusion Pumps

The LDPs are the high vacuum pumps installed in the INTL. Currently, three LDPs are considered to be installed in parallel per pumping port. The operating principle of diffusion pumps is based on the momentum transfer from a mercury vapor jet to the pumped gas. The mercury vapor jet is created by boiling mercury in an external boiler (e.g., using available process heat from the DIV cooling loop). The mercury vapor is then guided to the LDPs via a distribution system. Inside the LDP, one or multiple linear nozzle pipes are used to expand the mercury vapor into the pump body.

The expansion through the nozzle creates a supersonic mercury vapor jet that is directed in the pumping direction. Gas molecules diffuse into the jet(s) (the eponymous process), and on average, receive a positive momentum in the pumping direction by means of intermolecular collisions with the vapor. At the outlet, a BP is connected to remove the gas. Thermalization of the mercury vapor is prevented by actively cooling the outer walls of the LDP in order to condense incident mercury vapor. Like many other high vacuum pumps, diffusion pumps feature gas-type dependent pumping speeds. The main reason lies in the mass dependence of the thermal gas velocities.

TABLE II
Properties of the MBA Subsystem for Two Investigated Configurations

Property	Symbol	Unit	Configuration and Value	
			Vertical Mounting (a)	Inclined Mounting (b)
Inlet cross section (interface to MFPs)	$A_{2,in}$	m ²	3.04	
Outlet cross section (interface to LDPs)	$A_{2,out}$	m ²	1.68	
Transmission probability (TPMC, MOLFLOW+)	ω_2	1	0.0523	0.0556

A two-dimensional DSMC model of these pumps was established in previous work (see Teichmann and Day^[19] and Teichmann, Giegerich, and Day^[20]). The most important gas species in the exhaust gas mixture were simulated in Teichmann and Day^[19], and relative differences in the order of magnitude of about 10% were found between T₂ and D₂. For this reason, individual simulations were performed for each of the four most abundant gas species in the exhaust gas mixture, namely, He and the hydrogen isotopologues D₂, DT, and T₂. Two-dimensional DSMC simulations of a preliminary DEMO LDP design were performed under conditions estimated for the dwell and burn phases, respectively. An in-house modified version of the open-source code SPARTA^[21] was used to perform the DSMC simulations. Further details on the modifications are available in Teichmann, Giegerich, and Day.^[20] The actual performance of the three-dimensional pump was then estimated by simply scaling the two-dimensional results with the length of the LDP. The main properties and results are listed in Table III.

III.C. Hybrid Model

A loosely coupled hybrid model of the INTL high vacuum pumping system can be established by combining the subsystem simulation results using the Ansatz of Oatley as “mathematical glue.” Loosely coupled here means that the interaction between the subsystems is only considered in their mathematical combination using the Ansatz of Oatley and no feedback is interchanged between the simulations. Hybrid means that different calculation methods (TPMC and DSMC) are combined. Under the assumption of isothermal flow, the hybrid model prediction of the effective capture coefficient reads

$$\zeta_{\text{eff}} = \left[1 + \left(\frac{1}{\omega_1} - 1 \right) + \frac{A_{1,in}}{A_{2,in}} \left(\frac{1}{\omega_2} - 1 \right) + \frac{A_{1,in}}{A_{3,in}} \left(\frac{1}{\zeta_3} - 1 \right) \right]^{-1}, \quad (4)$$

where the transmission probabilities ω_i and the LDP capture coefficient ζ_3 depend on the subsystem configurations (MFP, MBA) and operating states (LDP), respectively.

IV. RESULTS

IV.A. Summary

A core benefit of the loosely coupled hybrid model is that a change in any subsystem configuration and corresponding performance only influences said subsystem and none of the other subsystems. Thus, the number of computations reduces to the sum of all subsystem configurations, whereas a tightly coupled model would require the computing of all system configurations individually. Transferred to the configurations investigated in the present work, this corresponds to 14 subsystem configurations (four MFPs, two MBAs, and eight LDPs) that have to be computed using TPMC or DSMC, respectively, whereas the total of 64 system configurations ($4 \times 2 \times 8$) follows from the mathematical coupling [see Eq. (4)] with only minimal additional computational effort. The total computational effort is therefore reduced by a factor of at least 4.6, and this efficiency gain is improved for an increasing number of subsystem configurations (as one would expect further along the subsystem design process).

The computed effective capture coefficients for all system configurations are collected in Table IV. Generally speaking, it can be seen that performance changes in the MBA (configurations a and b) and LDPs (depending on the gas type and operating phase) are dampened in the integrated system. The 6% improvement of the optimized MBA configuration b over the standard configuration a corresponds to an improvement of at most about 3% in the integrated system. The 8% difference

TABLE III

Properties and Performance of the LDP Subsystems Under Dwell- and Burn-Like Conditions with Respect to the Pumped Species

Property	Symbol	Unit	Pumped Gas and Value			
			He	D ₂	DT	T ₂
Inlet cross section per LDP	$A_{3,\text{in,LDP}}$	m ²	0.56			
Total inlet cross section (interface to MBA)	$A_{3,\text{in}}$	m ²	1.68 (= 3 · $A_{3,\text{in,LDP}}$)			
Terminal dwell inlet pressure (estimated)	$p_{3,\text{in,dwell}}$	Pa	2.5×10^{-4}			
Dwell compression ratio (approximate)	κ_{dwell}	1	4400	4400	4600	4800
Dwell capture coefficient (DSMC, SPARTA)	$\zeta_{3,\text{dwell}}$	1	0.243	0.238	0.249	0.258
Burn inlet pressure (estimated)	$p_{3,\text{in,burn}}$	Pa	0.5			
Burn compression ratio (approximate)	κ_{burn}	1	17	16	17	18
Burn capture coefficient (DSMC, SPARTA)	$\zeta_{3,\text{burn}}$	1	0.208	0.199	0.208	0.215

between the LDP capture coefficients for T₂ and D₂ is reduced to at most 2.5%. The dampening effect is amplified for system configurations that include MFP tubes with smaller diameters (configurations A and C). In order to identify the subsystems that bottleneck the integrated system, it is important to understand the relative sensitivities of the subsystems.

IV.B. Sensitivity Study

Due to the analytical coupling used to construct the hybrid model, it is possible to analyze the sensitivity of the system to its subsystems mathematically. Under the assumption that the layout of the system (i.e., the interfaces between subsystems) are fixed, which is reasonable as the space in the pumping ports is very limited, the transmission probabilities are the only determining factors. Therefore, the sensitivity of the system with respect to the property $\chi_i = \{\omega_i, \zeta_i\}$ of subsystem i follows as the partial derivative, namely,

$$\frac{\partial \zeta_{\text{eff}}}{\partial \chi_i} = \frac{A_{1,\text{in}}}{A_{i,\text{in}}} \cdot \left(\frac{\zeta_{\text{eff}}}{\chi_i} \right)^2. \quad (5)$$

The relative sensitivity around a reference point 0, characterized by the respective system configuration given by MFP and MBA configurations and gas species, is obtained by normalizing the partial derivative [Eq. 5] according to

$$\left. \frac{\partial \zeta_{\text{eff}}^*}{\partial \chi_i^*} \right|_0 = \frac{\chi_{i,0}}{\zeta_{\text{eff},0}} \cdot \left. \frac{\partial \zeta_{\text{eff}}}{\partial \chi_i} \right|_0 = \frac{A_{1,\text{in}}}{A_{i,\text{in}}} \cdot \frac{\zeta_{\text{eff},0}}{\chi_{i,0}}. \quad (6)$$

The relative sensitivities for all eight configurations of MFP and MBA during burn and dwell for DT as the pumped gas are depicted in Fig. 4.

As the species-dependent capture coefficients of the LDPs (see Table III) are dampened in the integrated system (see Table IV), the results can be considered representative for all gases in the exhaust mixture. The following discussion is equally true for burn (Fig. 4a) and dwell (Fig. 4b) as the subsystem sensitivities are nearly identical. Comparison of the relative sensitivities gives insight into the optimization potential of the individual subsystems.

For systems with MFP configurations A and C, which feature MFPs with smaller diameters, it is obvious that the system performance can basically only be improved by increasing the transmission probability (i.e., conductance) of the MFPs. The relative sensitivity of the subsystem containing the MFPs is more than five times higher than that of the other two subsystems in these configurations (A-a, A-b, C-a, and C-b), so that improvements of the other subsystems are practically nullified and are thus not worthwhile from an economic point of view. This is confirmed when comparing with MFP configurations B and D, which feature MFPs with larger diameters. In these cases the relative sensitivities of the subsystems are much closer, which implies that improvements of the subsystems can also have a significant impact on the integrated system.

In all configurations, the LDP capture coefficient is the least sensitive, which explains the dampening of the species dependency in the effective system capture coefficient. However, this also implies that there is little optimization potential for the LDPs, as illustrated in

TABLE IV

Effective Capture Coefficient of the INTL High Vacuum Pumping Train for Different Burn and Dwell Operating Conditions, Subsystem Configurations, and Pumped Gases

Tokamak Phase	MFP Configuration	MBA Configuration	ζ_{eff} Depending on Pumped Gas			
			He	D ₂	DT	T ₂
Dwell	A	a	0.00397	0.00397	0.00398	0.00398
		b	0.004	0.004	0.00401	0.00402
	B	a	0.0131	0.0131	0.0132	0.0132
		b	0.0135	0.0134	0.0135	0.0136
	C	a	0.00312	0.00312	0.00313	0.00313
		b	0.00314	0.00314	0.00315	0.00315
	D	a	0.0116	0.0116	0.0117	0.0117
		b	0.0119	0.0119	0.0119	0.012
Burn	A	a	0.00393	0.00392	0.00393	0.00394
		b	0.00397	0.00396	0.00397	0.00398
	B	a	0.0127	0.0126	0.0127	0.0128
		b	0.0131	0.0129	0.0131	0.0132
	C	a	0.0031	0.00309	0.0031	0.00311
		b	0.00312	0.00311	0.00312	0.00313
	D	a	0.0113	0.0112	0.0113	0.0114
		b	0.0116	0.0115	0.0116	0.0117

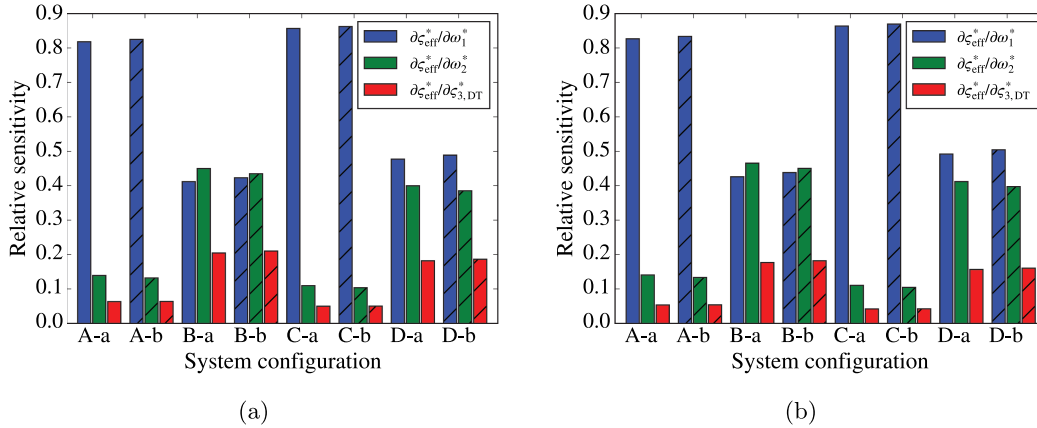


Fig. 4. Relative sensitivities of the subsystems on the effective system capture coefficient ζ_{eff} for DT during (a) burn and (b) dwell.

more detail in Fig. 5. Even for the more favorable MFP configurations B and D (larger tubes), the effective system capture coefficient only changes by approximately 16% (B) and 14% (D), respectively, if a LDP capture coefficient of unity is assumed (which is a theoretical boundary case much above practically achievable values) and by approximately 10% (B) and 9% (D), respectively, when assuming $\zeta_3 = 0.5$.

It is emphasized here again that the previous considerations are only valid under the assumption of free molecular flow that is taken in the TPMC models and the application of the Ansatz of Oatley. As this assumption leads to conservative estimations of the performance,

it is expected that the system performance will be improved in the transitional and viscous flow regimes and that the subsystem sensitivities will be more evenly distributed. With regard to the tokamak phases, this means that the earlier results should be considered realistic during dwell, but taken as lower limits during burn.

IV.C. Performance During Burn

During the tokamak burn phase, the DT fusion reaction is performed in the plasma in the torus. Both the DIRT and INTL pumping systems are active during this time. Within the existing uncertainties at the present design stage of EU-

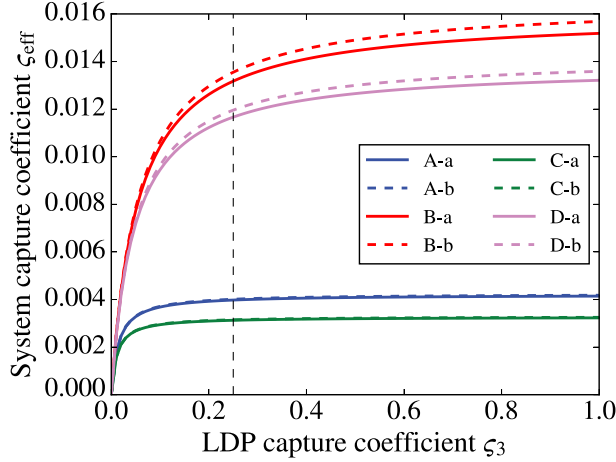


Fig. 5. Effective system capture coefficient ζ_{eff} as a function of the LDP capture coefficient ζ_3 for different system configurations.

DEMO, an indication of the upper bounds of the throughput that has to be handled by the vacuum systems during burn are given in Day et al.^[4]. We assume the total throughput is about $Q_{\text{total}}^* \leq 431 \text{ Pa m}^3 \text{ s}^{-1}$ (* : at reference temperature 273.15 K) with a composition of $x_{\text{Q}_2} \approx 0.99$ and $x_{\text{inert}} \approx 0.008$ (mostly helium ash). Under the assumption of a DIR recycling efficiency of 80%, about $Q_{\text{DIRL}}^* \leq 341 \text{ Pa m}^3 \text{ s}^{-1}$ of pure Q_2 are separated by the MFPs. Therefore $Q_{\text{INTL}}^* \leq 90 \text{ Pa m}^3 \text{ s}^{-1}$ have to be pumped by the INTL pumping system. Due to the extraction of pure Q_2 by the MFPs, the INTL composition changes to $x_{\text{Q}_2} \approx 0.96$ and $x_{\text{inert}} \approx 0.04$.

Based on the throughput, the required effective pumping speed per port can be estimated according to

$$S_{\text{eff,req}} = \frac{1}{N_{\text{ports}}} \cdot \frac{Q_{\text{INTL}}}{p_{\text{burn}}} \leq 6.3 \text{ m}^3 \text{ s}^{-1} , \quad (7)$$

where $N_{\text{ports}} = 10$ is the number of assumed pumping ports, $Q_{\text{INTL}} \leq 188 \text{ Pa m}^3 \text{ s}^{-1}$ (calculated from the reference value Q_{INTL}^* at the expected DIV temperature of 570 K) and $p_{\text{burn}} = 3 \text{ Pa}$ ^[3] is the assumed burn pressure in the sub-DIV region. It is emphasized here that there are still substantial uncertainties regarding the number of available pumping ports and the DIV performance, which is currently under reevaluation. The assumed values for N_{ports} and p_{burn} are examples to demonstrate the workflow, but might have to be revisited once more information on the DIV performance is known.

Now, the effective pumping speeds of the INTL pumping train can be estimated from the hybrid model results for the effective capture coefficient by means of Eq. (1). By inspection of Eq. (1), it is clear that the pumping speed is

proportional to \sqrt{m} , where m is the molecular mass of the considered species. When assuming thermal equilibrium between the hydrogen isotopologues, the INTL gas mixture during burn is composed of about 48% DT, 24% D_2 and T_2 , respectively, and 4% He (neglecting PEGs). For this reason, we estimate that assuming DT as the gas will give a good estimation for the entire mixture.

The effective pumping speeds for the different system configurations at 570 K are listed in Table V. Based on the hybrid model results, all MFP configurations are capable of providing the required effective pumping speed (per port) of $6.3 \text{ m}^3 \text{ s}^{-1}$. Configurations B ($\approx 28 \text{ m}^3 \text{ s}^{-1}$) and D ($\approx 25 \text{ m}^3 \text{ s}^{-1}$) include a comfortable safety factor in the range of 4 to 4.5. However, as stated before, the hybrid model is based on the assumption of free molecular flow. It therefore is likely that the actual pumping speeds would be higher during burn conditions, as the flow regime is in the transitional to viscous regime.

IV.D. Performance During Dwell

Contrary to the burn phase, the dwell phase is transient. The torus is pumped down from burn conditions to the terminal dwell pressure. This pressure has to be significantly lower than the burn pressure in order to prepare for the next plasma ignition. For the MFPs, the most likely scenario is that they can support the INTL pumping system at the beginning of the pump-down phase. However, in order to provide a conservative estimation, we will assume that only the INTL pumping train is active during dwell. Similar to the considerations for the burn phase, we assume that the effective pumping speed of DT is a good estimate of the mixture pumping speed. The results of the hybrid model are given in Table V.

The pump-down can then be described by the differential equation

$$V \cdot \frac{dp}{dt} = -N_{\text{ports}} \cdot S_{\text{eff}} \cdot p + Q_{\text{dwell}} , \quad (8)$$

where $V \approx 6400 \text{ m}^3$ is the torus volume^[22] and Q_{dwell} is the gas load during dwell. Equation (8) can be integrated between the start/burn p_0 and terminal p_1 pressures to obtain an expression for the pump-down time Δt :

$$\Delta t = -\frac{V}{N_{\text{ports}} \cdot S_{\text{eff}}} \cdot \ln \left(\frac{p_1 \cdot N_{\text{ports}} \cdot S_{\text{eff}} - Q_{\text{dwell}}}{p_0 \cdot N_{\text{ports}} \cdot S_{\text{eff}} - Q_{\text{dwell}}} \right) . \quad (9)$$

TABLE V

Effective DT Pumping Speed $S_{\text{eff,DT}}$ of the INTL High Vacuum Pumping Train for Different Subsystem Configurations During Dwell and Burn Phases at $T = 570$ K

Tokamak Phase	MFP Configuration	MBA Configuration	$S_{\text{eff,DT}}$ ($\text{m}^3 \text{s}^{-1}$)
Dwell	A	a	8.65
		b	8.73
	B	a	28.7
		b	29.5
	C	a	6.80
		b	6.85
	D	a	25.4
		b	26.0
Burn	A	a	8.56
		b	8.63
	B	a	27.7
		b	28.4
	C	a	6.75
		b	6.79
	D	a	24.6
		b	25.2

The pressures in the sub-DIV volume are assumed as $p_0 = 3$ Pa and $p_1 = 2 \times 10^{-3}$ Pa.^[3] We emphasize here that these are subject to change due to the uncertainties regarding the DIV performance. The gas load during dwell is comprised of two main sources: outgassing from the first wall and leakage into the torus. It is expected that the former will dominate the outgassing rate. Day et al.^[4] estimated an integral protium outgassing rate for tungsten of approximately $0.15 \text{ Pa m}^3 \text{ s}^{-1}$ (at 573.15 K). However, as also noted by them, this does not include plasma-driven implantation and neutron damage, which are expected to alter the magnitude and composition of the outgassing gas over the lifetime of the machine. Therefore, it should be considered as a lower limit. Due to these uncertainties, we kept the outgassing rate as a free parameter and studied its influence on the pump-down time. The results for the different system configurations are depicted in Fig. 6.

The targeted pump-down time of $\Delta t < 600$ s (see Day et al.^[4]) is only realistically achieved for system configurations B- $\{a,b\}$ and D- $\{a,b\}$. Configurations C- $\{a,b\}$ cannot meet the target time even in the unphysical limit of no gas load ($Q_{\text{dwell}} = 0$). While configurations A- $\{a,b\}$ can meet the target pump-down time theoretically, this is only possible for outgassing rates significantly below the lower limit represented by the expected protium outgassing rate.

Furthermore, Fig. 6 illustrates that there is a parameter window in which, after a critical outgassing rate is exceeded, it is impossible to pump down to the

targeted terminal pressure even when relaxing the pump-down time requirement. This critical outgassing rate is found by solving Eq. (8) in steady state (i.e., setting $dp/dt = 0$). For the present system architectures, this limit lies at approximately $0.58 \text{ Pa m}^3 \text{ s}^{-1}$ and $0.51 \text{ Pa m}^3 \text{ s}^{-1}$ for MFP configurations B and D, respectively. It is therefore of vital importance that better estimations of the outgassing rate and the necessary terminal dwell pressure become available. Additionally, a different arrangement of the pumps may have to be considered (e.g., switching MFP and LDP positions) so as to provide a higher conductance, and by that, to move the operational constraints.

V. SUMMARY AND OUTLOOK

We introduced a hybrid model of the EU-DEMO INTL high vacuum pumping system. The hybrid model was developed based on the loose coupling of individual models of three subsystems: duct including MFPs, MBA, and LDPs. The coupling was achieved by applying the Ansatz of Oatley. While not expected to be as accurate as a direct simulation of the combined INTL high vacuum system, the presented hybrid model has distinct advantages, as illustrated. First, usage of individual simulation models for the subsystems allows for employing the most suitable method and tool for the individual subsystems, which enables more efficient parametric optimization of these systems. Second, coupling by the analytical Ansatz

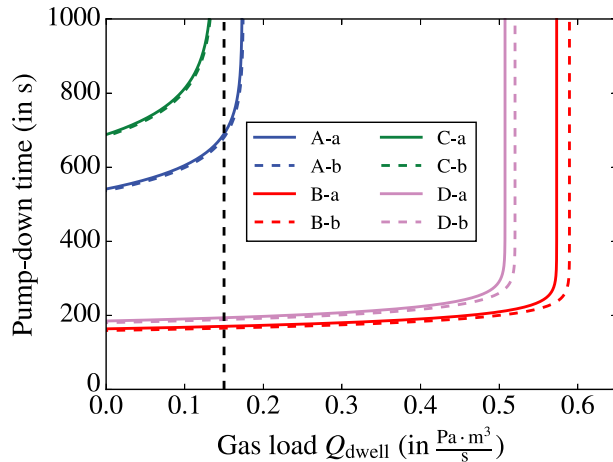


Fig. 6. Dwell pump-down time Δt as a function of the dwell gas load Q_{dwell} for the different INTL system configurations.

of Oatley creates the possibility of analyzing the sensitivities of the subsystem performances on the system performance mathematically. This gives insight into bottleneck subsystems, which have the highest optimization potential and optimization limitations.

In the present work, two different three-dimensional TPMC programs were used to simulate the transmission probabilities of the duct and baffle adapter, while two-dimensional DSMC was used to estimate the capture coefficient of the LDPs. Four different MFP configurations were compared. The impact of the inherent species-dependent performance of the LDPs on the effective system performance was analyzed. We found that the effective system performance was not very sensitive to the LDP performance in the configurations investigated.

The hybrid model was then exploited to predict the performance of the integrated INTL pumping system during the tokamak operating phases (burn and dwell) with respect to four different MFP configurations and two different MBA configurations. Comparing the effective pumping speed to the upper limits of the required pumping speed during burn, we found that all eight configurations performed as required (four even with a comfortable safety factor). Regarding the dwell phase, we used the model to estimate the pump-down time as a function of the gas load (assumed to be dominated by outgassing from the first wall). We found that the same four configurations can meet the required pump-down time. However, it was also found that the critical outgassing rate, above which the targeted terminal pressure cannot be reached, lies in the same order of magnitude as the expected protium outgassing rate alone.

The following points should be addressed in future research. It has to be tested if and how the DIV can be included in the hybrid model to extend the predictions from the sub-DIV volume to the actual plasma chamber. Additionally, the study can be extended by considering further exhaust gas mixture constituents (e.g., PEGs) once more reliable information on the expected amounts becomes available. Furthermore, the results of the loosely coupled hybrid model should, if possible, be compared to a full simulation of the INTL system. However, it is noted that this is currently not feasible because it would require a full three-dimensional DSMC model of the system, which cannot be computed in reasonable timescales even on up-to-date supercomputers, not to mention that the full model would have to reflect an existing three-dimensional design, which is not existing at the current concept design stage.

Ad interim, the approach shown in this paper serves to provide a helpful and consistent description to support design development. Regarding the performance during dwell, it is recommended to establish/improve the estimation of the outgassing rate and the terminal dwell pressure. Last, it is recommended to perform a broader study with a systematic variation of the pump arrangements to assess if the dwell performance can be improved.

Acknowledgments

Simulations were partially performed on the EUROfusion high-performance computer Marconi-Fusion. The authors gratefully acknowledge the resources allocated to projects VAC ND and LDP KIT. The authors would like to thank Ralf Müller for his help in preparing the CAD drawings.

Disclosure Statement

No potential conflict of interest was reported by the authors.

Funding

This work was carried out within the framework of the EUROfusion Consortium, funded by the European Union via the Euratom Research and Training Programme [grant agreement no. 101052200—EUROfusion]. The views and opinions expressed, however, are those of the authors only and do not necessarily reflect those of the European Union or the European Commission. Neither the European Union nor the European Commission can be held responsible for them.

ORCID

Tim Teichmann  <http://orcid.org/0000-0001-6957-7092>

References

1. C. DAY and T. GIEGERICH, “The Direct Internal Recycling Concept to Simplify the Fuel Cycle of a Fusion Power Plant,” *Fusion Eng. Des.*, **88**, 6–8, 616 (2013); <https://doi.org/10.1016/j.fusengdes.2013.05.026>.
2. T. GIEGERICH and C. DAY, “The KALPUREX-Process—A New Vacuum Pumping Process for Exhaust Gases in Fusion Power Plants,” *Fusion Eng. Des.*, **89**, 7–8, 1476 (2014); <https://doi.org/10.1016/j.fusengdes.2014.03.082>.
3. T. GIEGERICH et al., “Preliminary Configuration of the Torus Vacuum Pumping System Installed in the DEMO Lower Port,” *Fusion Eng. Des.*, **146**, B, 2180 (2019); <https://doi.org/10.1016/j.fusengdes.2019.03.147>.
4. C. DAY et al., “The Pre-concept Design of the DEMO Tritium, Matter Injection and Vacuum Systems,” *Fusion Eng. Des.*, **179**, 113139 (2022); <https://doi.org/10.1016/j.fusengdes.2022.113139>.
5. T. L. HO, “Speed, Speed Factor and Power Input of Different Designs of Diffusion Pumps, and Remarks on Measurements of Speed,” *Physics*, **2**, 386 (1932); <https://doi.org/10.1063/1.1745064>.
6. D. H. DAVIS, “Monte Carlo Calculation of Molecular Flow Rates Through a Cylindrical Elbow and Pipes of Other Shapes,” *J. Appl. Phys.*, **31**, 7, 1169 (1960); <https://doi.org/10.1063/1.1735797>.
7. G. A. BIRD, *Molecular Gas Dynamics and the Direct Simulation of Gas Flows*, No. 42 in Oxford Engineering Science Series, Oxford University Press Inc. (1994).
8. C. W. OATLEY, “The Flow of Gas Through Composite Systems at Very Low Pressures,” *Br. J. Appl. Phys.*, **8**, 1, 15 (1957); <https://doi.org/10.1088/0508-3443/8/1/305>.
9. L. FÜSTÖSS and G. TÓTH, “The Problem of the Compounding of Transmission Probabilities for Composite Systems,” *J. Vac. Sci. Technol.*, **9**, 4, 1214 (1972); <https://doi.org/10.1116/1.1317015>.
10. L. FÜSTÖSS and G. TÓTH, “The Resistance Concept and the Dynamical Characterization of Molecular Gas Flow,” *Vacuum*, **40**, 1, 43 (1990); [https://doi.org/10.1016/0042-207X\(90\)90115-F](https://doi.org/10.1016/0042-207X(90)90115-F).
11. K. JOUSTEN, “Molekulare Strömung von Gasen,” Chap. 8 in *Handbuch Vakuumtechnik*, 12th ed., K. JOUSTEN, Ed., pp. 171–193, Springer (2018).
12. V. HAUER and C. DAY, “Conductance Modelling of ITER Vacuum Systems,” *Fusion Eng. Des.*, **84**, 2, 903 (2009); <https://doi.org/10.1016/j.fusengdes.2008.12.115>.
13. D. A. KARPOV et al., “Vacuum Pumping System of TRT,” *Plasma Phys. Rep.*, **47**, 12, 1267 (2021); <https://doi.org/10.1134/S1063780X21120023>.
14. B. J. PETERS and C. DAY, “Analysis of Low Pressure Hydrogen Separation from Fusion Exhaust Gases by the Means of Superpermeability,” *Fusion Eng. Des.*, **124**, 696 (2017); <https://doi.org/10.1016/j.fusengdes.2017.05.124>.
15. B. J. PETERS, “Development of a Hydrogen-Selective Vacuum Pump on the Basis of Superpermeation,” PhD Thesis, Department of Mechanical Engineering, Karlsruhe Institute of Technology (2020).
16. X. LUO and C. DAY, “3D Monte Carlo Vacuum Modeling of the Neutral Beam Injection System of ITER,” *Fusion Eng. Des.*, **85**, 7–9, 1446 (2010); <https://doi.org/10.1016/j.fusengdes.2010.04.002>.
17. X. LUO et al., “Assessment of the JT-60SA Divertor Cryopump Performance,” *Fusion Eng. Des.*, **136**, 467 (2018); <https://doi.org/10.1016/j.fusengdes.2018.02.099>.
18. R. KERSEVAN and J.-L. PONS, “Introduction to MOLFLOW+: New Graphical Processing Unit-Based Monte Carlo Code for Simulating Molecular Flows and for Calculating Angular Coefficients in the Compute Unified Device Architecture Environment,” *J. Vac. Sci. Technol., A*, **27**, 4, 1017 (2009); <https://doi.org/10.1116/1.3153280>.
19. T. TEICHMANN and C. DAY, “Particle Simulation of Linear Diffusion Pumps for DEMO Torus Exhaust Pumping,” *Fusion Eng. Des.*, **169**, 112694 (2021); <https://doi.org/10.1016/j.fusengdes.2021.112694>.
20. T. TEICHMANN, T. GIEGERICH, and C. DAY, “Simulation of Mercury-Driven Diffusion Pumps for Torus Exhaust Pumping,” *IEEE Trans. Plasma Sci.*, **50**, 11, 4459 (2022); <https://doi.org/10.1109/TPS.2022.3202083>.
21. S. J. PLIMPTON et al., “Direct Simulation Monte Carlo on Petaflop Supercomputers and Beyond,” *Phys. Fluids*, **31**, 8, 086101 (2019); <https://doi.org/10.1063/1.5108534>.
22. M. D’ONORIO and G. CARUSO, “Pressure Suppression System Influence on Vacuum Vessel Thermal-Hydraulics and on Source Term Mobilization During a Multiple First Wall–Blanket Pipe Break,” *Fusion Eng. Des.*, **164**, 112224 (2021); <https://doi.org/10.1016/j.fusengdes.2020.112224>.